Secondary Ion Mass Spectrometry analysis of metal oxides using 70 keV argon, carbon dioxide and water gas cluster ion beams

DOI:
10.1116/6.0002591

Document Version
Accepted author manuscript

Secondary Ion Mass Spectrometry analysis of metal oxides using 70 keV argon, carbon dioxide and water gas cluster ion beams

Running title: GCIB SIMS of metal oxides

Running Authors: Alsaedi et al.

A.H. Alsaedi, A.S. Walton and N.P. Lockyer [a)]

Photon Science Institute, Department of Chemistry, University of Manchester, Oxford Rd., Manchester M13 9PL, U.K.

[a)] Electronic mail: nick.lockyer@manchester.ac.uk

Manganese (II) oxide (MnO), manganese (IV) oxide (MnO_2), cobalt (II,III) oxide (Co_3O_4) and nickel (II) oxide (NiO) were analysed with time-of-flight secondary ion mass spectrometry using 70 keV gas cluster ion beams. The obtained mass spectra are influenced by projectile chemistry and to a lesser extent velocity. Gas cluster ion beams containing CO_2 or H_2O enhanced the relative yield of metal oxide and metal hydroxide secondary ions compared to beams containing only Ar. For all gas cluster ion beams tested, steady state ion ratios $[M_xO_y]^+/[M_x]^+$ were reached. For manganese oxides, the $[Mn_xO_y]^+/[Mn_x]^+$ ratio reflected the metal oxidation state whereas the $[Mn_xO_yH_z]^+/[Mn_x]^+$

ion ratios did not. This study demonstrates that Secondary Ion Mass Spectrometry using 70 keV gas cluster ion beams provides a novel approach to the quantitative analysis of the surface and sub-surface regions of metal oxides related to energy-storage materials.

I. INTRODUCTION

Elemental analysis and molecular speciation are essential tools in solid state physics and in the development of next-generation electronic materials *e.g.* battery components.[1,2,3] Secondary Ion Mass Spectrometry (SIMS) is a powerful technique for probing the composition of a material's surface and subsurface, providing 2D and 3D distributions of chemical species. Time-of-Flight (ToF-) SIMS allows non-targeted analysis of a wide range of chemical species extending to 1000s mass units with high specificity and sensitivity. Molecular speciation analysis is possible with ToF-SIMS, from the relative signal intensities of molecular ions including $[M_xO_y]^+$ from metal oxides[4] which are relevant to energy storage devices.

Gas cluster ion beams (GCIBs) comprising projectiles of 1000s of atoms accelerated to keV energies are important tools in materials processing *e.g.* of semiconductor surfaces[5] and as primary ion sources for SIMS analysis.[6] The dynamics of GCIB impact on a surface leads to high sputter yield of molecular secondary species and low chemical damage as a result of low energy penetration into the bulk.[7] This facilitates molecular depth profiling with improved depth resolution (<10 nm) compared with small

cluster/atomic primary ion beams.[8] The application of relatively low energy GCIBs to sputter profile organic materials in combination with X-ray Photoelectron Spectroscopy (XPS) is an established methodology.[9] ToF-SIMS is complementary to XPS for materials surface and interface analysis, offering enhanced specificity, sensitivity and lateral resolution, albeit with less straightforward quantification.[10,11] One example is all-solid-state batteries where it is important to characterize ion migration and metal oxidation states in the so-called 'solid electrolyte interphase' (SEI) to monitor electrode degradation. [3,10,11,12]

The application of GCIB SIMS has focused to-date on the analysis of organic samples including biological cells and biomaterials[13]. In contrast, applications in inorganic analysis have hardly been explored, partly because the secondary ion yield from inorganic materials is low using GCIB projectiles with <20 keV impact energy. However, the impressive depth-profiling capabilities of GCIB SIMS makes it an attractive prospect for inorganic surface and interface analysis, where high depth resolution and low inter-layer mixing are required. The size and chemistry of the constituent GCIB species affects the sputtering process and provides the opportunity to optimize the SIMS analysis *i.e.* depth resolution and secondary ion (SI) yield. Moreover, the capability of GCIB sputtering to produce larger molecular clusters provides enhanced opportunity for quantitative speciation analysis.[14,15] For quantitative determination of the oxidation state of component materials, it is essential to understand the effect of the primary ion beam on the resulting mass spectrum. For example argon GCIBs have been reported to induce chemical modification at 6 eV/atom in certain inorganic semiconductors.[16] In this paper we present a high-energy GCIB SIMS study of a series

of metal oxides. The aim is to reveal how the relative yield of diagnostic secondary ions which can be used for speciation analysis of mixed metal oxides is affected to the choice of GCIB size, chemistry and ion dose.

II. EXPERIMENTAL

A. Sample preparation

Samples were selected that are of direct relevance to the analysis of $LiNi_xMn_yCo_zO_2$ (*NMC*) lithium-ion batteries. Manganese (II) oxide (MnO), manganese (IV) oxide (MnO_2), cobalt (II,III) oxide (Co_3O_4) and nickel (II) oxide (NiO) were analysed as powders in this study. Apart from NiO (PI-KEM Ltd, UK), all samples were obtained from Sigma Aldrich, UK. Particles sizes as supplied were as follows: MnO 250 µm, MnO_2 <10 µm, Co_3O_4 <50 nm and NiO <2 µm. Samples were prepared in a glovebox and pressed onto conductive carbon tape before mounting for SIMS analysis.

B. Gas Cluster Ion Beams

For this study a 70 keV GCIB (Ionoptika Ltd, U.K.) was used. The source is capable of generating $(Ar)_n$, $(CO_2)_n$ or $(H_2O)_n$ clusters as described previously.[17,18] The $(CO_2)_n$ beam was generated using a feed gas of 12% CO_2 in Ar. Lee *et al.* measured the composition of Ar/CO_2 at different CO_2:Ar mole fraction and found that at a mole fraction of 5% of CO_2, 38% of the cluster is composed of CO_2, and when the CO_2 mole fraction is increased to 10%, CO_2 is the dominant species in the cluster beam.[19] Cluster size selection is performed by a Wien filter. Here we used relatively small clusters ($1000<n<3000$) to optimise the secondary ion yield of relatively low mass secondary ions. A key parameter in sputtering dynamics is the energy per nucleon (E/m) of the

projectile *i.e*. cluster velocity. We therefore chose a range of cluster sizes to enable the influence of *E*/*m* as well as cluster chemistry to be determined. It should be noted that Ar and CO_2 have closely related mass so to a first approximation GCIBs of these components with identical *n* will have comparable *E*/*m* values.

C. ToF-SIMS Analysis

ToF-SIMS analysis was performed using a J105 3D chemical Imager (Ionoptika Ltd, UK).[20] Prior to data acquisition, samples were cleaned of surface contamination within an area 500 × 500 μm^2 using GCIB sputter etching with the analysis beam to a dose 1.5 × 10^{12} ion/cm^2. Data acquisition involved a series of analyses (N=20−40) from 250 × 250 μm^2 areas within the cleaned region, with each analysis using a GCIB dose of 4.5 × 10^{12} ion/cm^2. Triplicate analyses were performed with the $(CO_2)_n$ GCIB, and duplicate analyses using the $(H_2O)_n$ GCIB, using a fresh area for each analysis. For reference only, steady-state SI yields using a 40 keV C_{60}^+ ion beam are included.

III. RESULTS AND DISCUSSION

A. Comparison of $(Ar)_n$ and $(CO_2)_n$ GCIBs for the detection of metal oxide signals $[M_xO_y]^+$

To compare the relative secondary ion yields of metal oxide species, the peak intensity $[M_xO_y]^+$ relative to $[M_x]^+$ (x and y = 1 or 2) was measured for different Ar/CO_2 GCIBs (n = 1000, 2000 or 3000) from MnO, MnO_2, NiO and Co_3O_4 samples. To explore primary ion dose-dependency, relative SI yields were measured from MnO as a function of GCIB dose as the surface is sputter-etched (Fig. 1). For the $(Ar)_n$ beams a steady state in the

$[MnO]^+/[Mn]^+$ ratio is reached after ~2×10^{13} ion/cm^2, whereas for the $(CO_2)_n$ beams the steady state dose is ~ 4×10^{13} ion/cm^2.

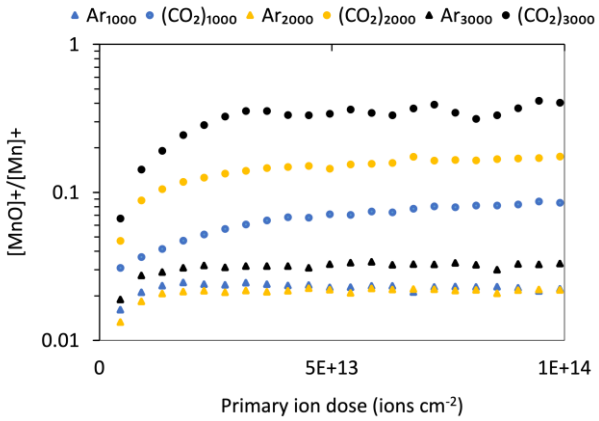

FIG. 1. The effect of the primary ion dose of Ar_n and $(CO_2)_n$ (n = 1000 − 3000) on the secondary ion yield ratio $[MnO]^+/[Mn]^+$ from MnO.

It might be expected that GCIBs with molecular constituents (in this case CO_2) would exhibit a reduced sputter yield compared with atomic GCIBs of the same velocity, as some of the impact energy is directed into breaking inter- and intramolecular attractions *i.e.* chemical bonds and dipole-dipole interactions. However, sputter yields also scale with projectile velocity[21,22] whereas the $(CO_2)_n$ data in Fig. 1. shows that a steady state in the $[MnO]^+/[Mn]^+$ ratio is reached at a comparable dose for each $(CO_2)_n$ beam. We therefore suggest that this SI yield ratio is a reflection not only of removing surface contamination, but also of chemical reactions between surface moieties and components of the GCIB. This conclusion is supported by different steady-state yield ratios from the $(CO_2)_n$ beams as discussed below.

Representative SIMS spectra of MnO_2 obtained under steady-state sputtering from $(Ar)_n$ and $(CO_2)_n$ GCIBs are shown in Fig. 2, with signal intensity normalised to the Mn^+ peak using $(Ar)_{1000}$. For both $(Ar)_n$ and $(CO_2)_n$ GCIBs the highest SI yields (measured per primary ion) from this sample are observed with the n = 2000 projectile. A general observation is that higher mass secondary ions are favoured by larger, slower cluster projectiles and by those containing $(CO_2)_n$. A comparison of SIMS spectra from MnO and MnO_2 using the $(CO_2)_{3000}$ GCIB is shown in Fig. S1. SI yield ratios from each sample were measured in the steady-state dose regime from each GCIB. The $(Ar)_n$ GCIBs result in a low SI yield of $[MO]^+$ relative to $[M]^+$ (Fig. 3). Switching to $(CO_2)_n$ GCIBs of comparable (E/m) results in enhancement of $[MO]^+/[M]^+$ ratio by a factor ×4−5. For both types of projectile, larger clusters with lower (E/m) increase the relative SI yield of $[MO]^+$. The SI yield $[M_2O_2]^+$ relative to $[M_2]^+$ for each of the samples is shown in Fig. 4. The $[M_2O_2]^+/[M_2]^+$ ratio shows no significant dependence on (E/m) for the $(Ar)_n$ GCIBs and no enhancement with the $(CO_2)_{1000}$ beam. However the larger $(CO_2)_n$ projectiles (n = 2000 or 3000) produce a significant increase in relative $[M_2O_2]^+$ yield from each sample.

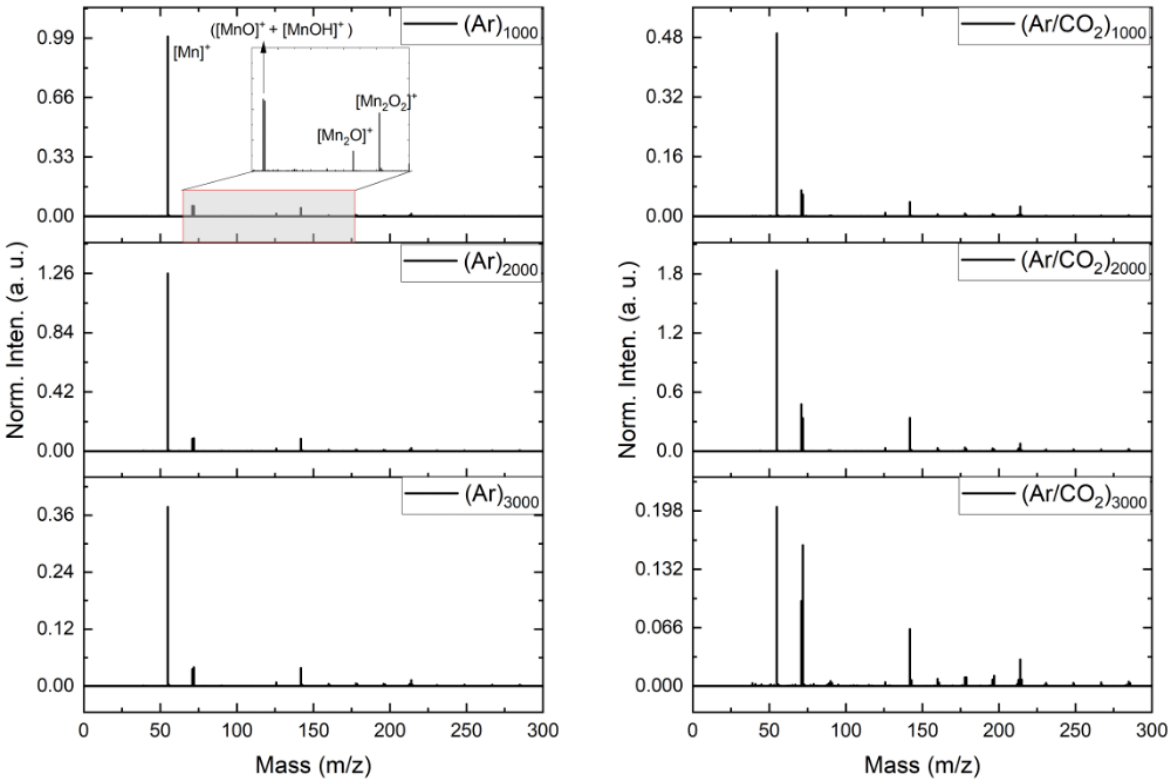

FIG. 2. Steady-state SIMS spectra of MnO_2 obtained with primary ion beams of Ar_n and $(CO_2)_n$ (n = 1000 − 3000). All spectra were acquired with the same primary ion dose. The intensity scale is normalized to the spectrum obtained with the Ar_{1000} GCIB.

Our data are consistent with oxygen transfer between $(CO_2)_n$ GCIBs and metal oxides samples from dissociation of CO_2 in the projectiles. Hua *et al*. showed that the C-O bond in $(CO_2)_n$ projectiles undergoes dissociation if the projectile energy per molecule is >5 eV/*n*, enhancing the oxides peaks in the SIMS analysis of gold.[18] Our data spans the range 23-70 eV/*n*. Increased metal oxide signals with increased cluster size may result from the higher probability of the interaction between the surface sample and oxygen that is generated from CO_2 dissociation, either because the larger projectile

contains more oxygen and/or is moving slower so projectile constituents will spend a longer time in the region of the surface after projectile shattering.

Comparing data from manganese (II) oxide and manganese (IV) oxide shows a ×2−3 increase in ion ratios from the higher metal oxidation state, demonstrating the capability of these high-energy GCIBs to provide speciation analysis.

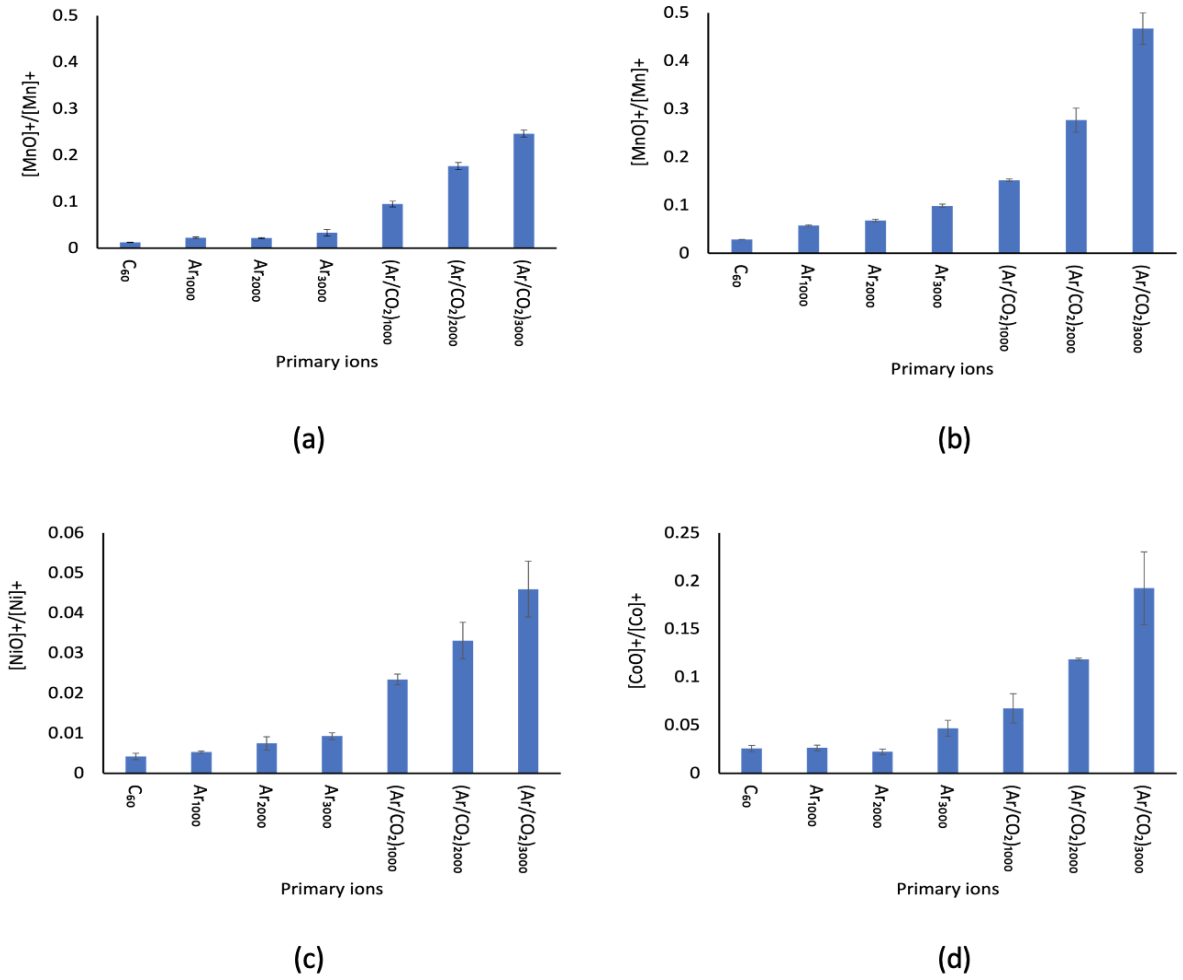

FIG. 3. The effect of the primary ions C_{60}, Ar_n and $(CO_2)_n$ (n = 1000, 2000, 3000) on the secondary ion yield ratio (MO^+/M^+), where M = metal and MO = metal oxide from (a)

MnO, (b) MnO_2, (c) NiO and (d) Co_3O_4. The error bars represent the standard deviation of analysis obtained from three different areas.

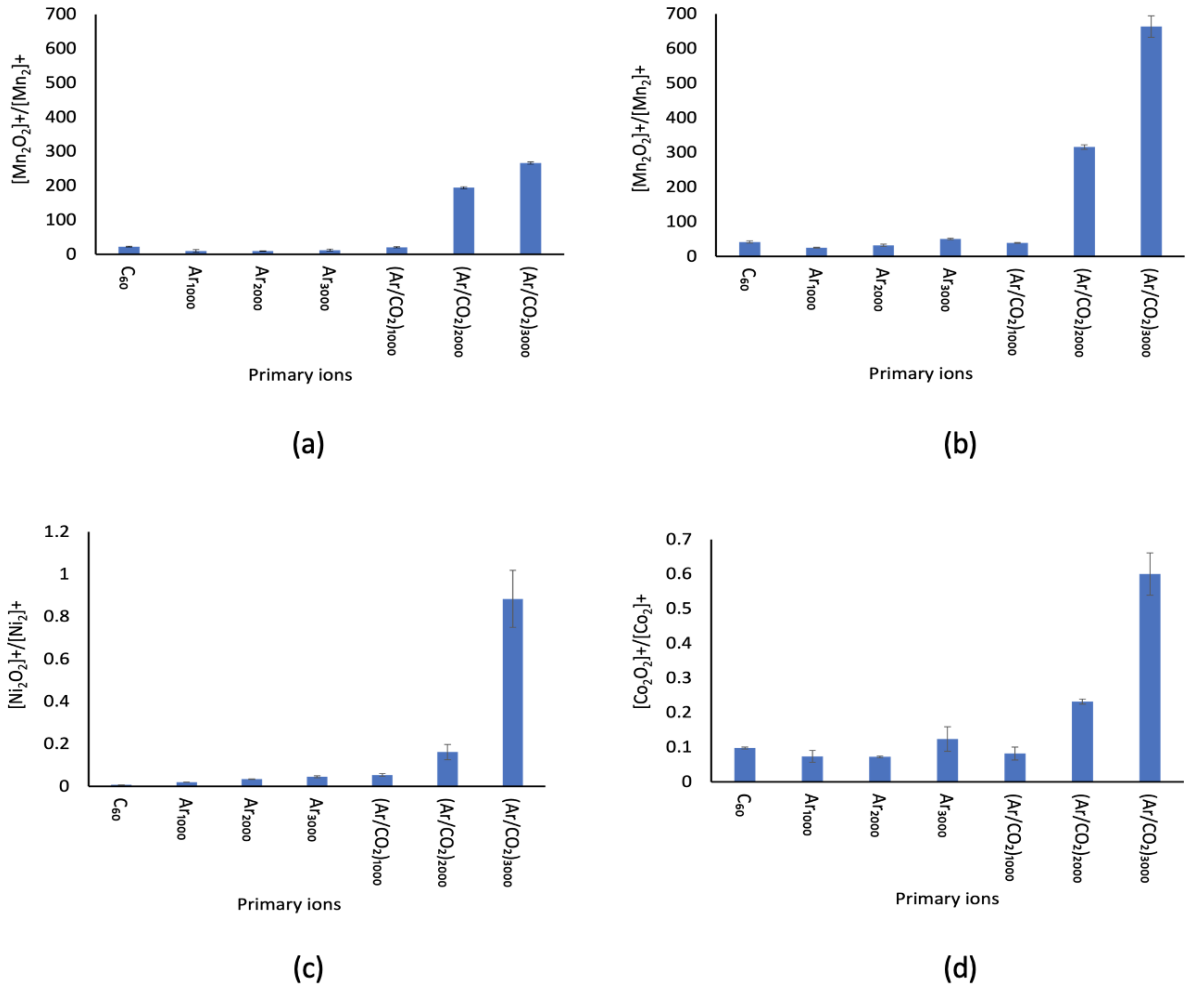

FIG. 4. The effect of the primary ions C_{60}, Ar_n and $(CO_2)_n$ (n = 1000, 2000, 3000) on the secondary ion yield ratio $[M_2O_2]^+/[M_2]^+$ where M = metal and M_2O_2 = metal oxide from the samples (a) MnO, (b) MnO_2, (c) NiO and (d) Co_3O_4. The error bars represent the standard deviation of analysis obtained from three different areas.

To investigate further the mechanism of oxide ion enhancement with (CO_2) GCIBs we compared three different projectile cluster sizes at the same *E*/*m* of 0.53 eV/u. The data in Fig. 5 show a very similar plateau in $[MO^+]/[M^+]$ ion yield ratio. This implies that cluster velocity is more important than cluster size in determining projectile-mediated SI formation reactions, under the conditions applied here (23-70 keV, n = 1000-3000).

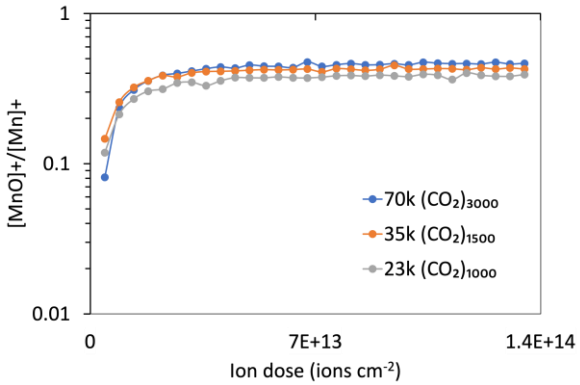

FIG. 5. The effect of the primary ion dose of $(CO_2)_n$ (n = 1000 − 3000) projectiles of fixed *E*/*m* = 0.53 eV/u on the secondary ion yield ratio $[MnO]^+/[Mn]^+$ from MnO_2 sample.

B. Comparison of $(Ar)_n$ and $(H_2O)_n$ GCIBs for the detection of metal hydroxide signals $[M_xO_yH_z]^+$

Using $(H_2O)_n$ GCIBs is known to enhance the formation of $[M+H]^+$ in the SIMS analysis of organics.[17] However, the effect of water GCIBs on inorganic materials has not been reported previously. To investigate any effect on adduct ion yields from metal oxides, signal ratios of $[M_xO_yH_z]^+/[M_x]^+$ were measured for $(Ar)_n$ and $(H_2O)_n$ GCIBs on each sample. Again, C_{60} SIMS data are included for reference.

Fig. 6. shows relative SI yields $[MnOH]^+/[Mn]^+$ from MnO using $(Ar)_{1000}$, $(Ar)_{2000}$, $(Ar)_{3000}$, $(H_2O)_{1200}$ and $(H_2O)_{3000}$ as a function of primary beam dose. As before, the sample areas were pre-etched with 1.5×10^{12} ion/cm^2 of the analytical beam immediately prior to data collection. The $(Ar)_n$ data shows an initial decrease in ion ratio followed by a plateau after a dose ~2×10^{13} ion/cm^2 (in agreement with Fig. 1). Each $(Ar)_n$ GCIB provides a very similar ratio $[MnOH]^+/[Mn]^+$. This result is consistent with a sample which is partly hydrated in the surface region due to atmospheric exposure. Hard X-ray Photoelectron Spectroscopy analysis of the same samples (Fig S3) demonstrates that sample heating is required to remove hydroxide signals from the surface – no heating was employed prior to SIMS analysis. See supplementary material at [URL will be inserted by AIP Publishing] for discussion of the XPS results. Both $(H_2O)_n$ GCIBs show an initial small rise followed by a plateau in the ion ratio, which is between one and two orders of magnitude greater than that observed for the $(Ar)_n$ GCIBs.

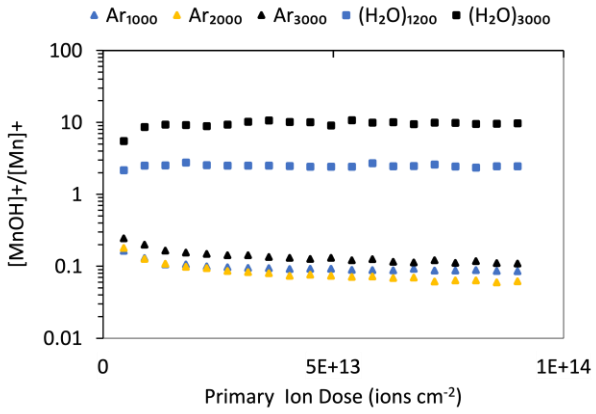

FIG. 6. The effect of the primary ion dose of Ar_n and $(H_2O)_n$ (n = 1000−3000) on the secondary ion yield ratio $[MnOH]^+/[Mn]^+$ from a sample of MnO.

Fig. 7 shows the $[M_xO_yH_z]^+/[M_x]^+$ SI yield ratio measured for C_{60}, $(Ar)_n$ and $(H_2O)_n$ GCIBs on each sample. As before, the $(Ar)_n$ data show no significant differences but the $(H_2O)_n$ GCIBs provide large increases in the hydroxide-containing adducts, an order of magnitude increase in SI yield ratio compared with $(Ar)_n$ projectiles of comparable (E/m).

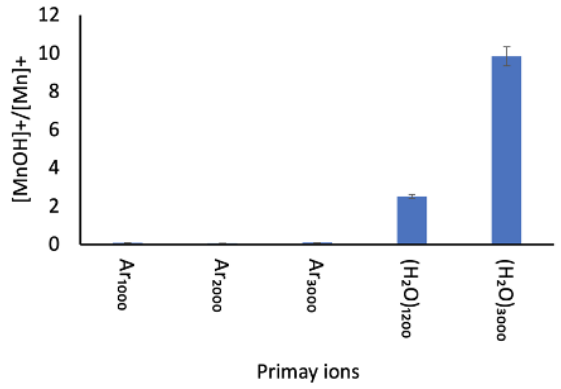
[MnOH]+/[Mn]+
12
10
8
6
4
2
0
Ar1000
Ar2000
Ar3000
(H2O)1200
(H2O)3000
Primay ions

(a)

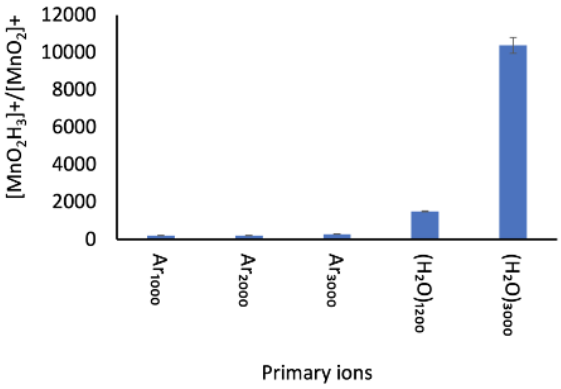
[MnO2H3]+/[MnO2]+
12000
10000
8000
6000
4000
2000
0
Ar1000
Ar2000
Ar3000
(H2O)1200
(H2O)3000
Primary ions

(b)

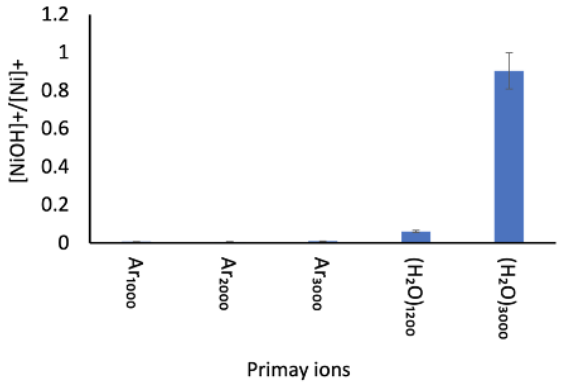
[NiOH]+/[Ni]+
1.2
1
0.8
0.6
0.4
0.2
0
Ar1000
Ar2000
Ar3000
(H2O)1200
(H2O)3000
Primay ions

(c)

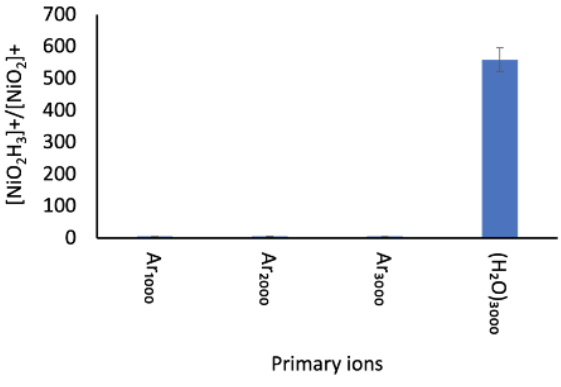
[NiO2H3]+/[NiO2]+
700
600
500
400
300
200
100
0
Ar1000
Ar2000
Ar3000
(H2O)3000
Primary ions

(d)

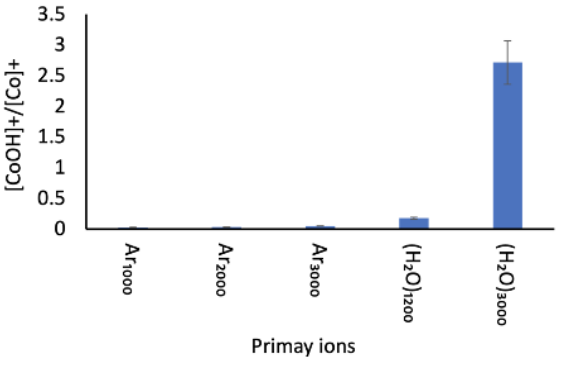
[CoOH]+/[Co]+
3.5
3
2.5
2
1.5
1
0.5
0
Ar1000
Ar2000
Ar3000
(H2O)1200
(H2O)3000
Primay ions

(e)

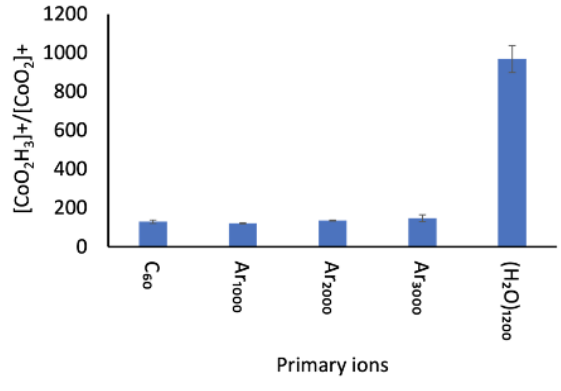
[CoO2H3]+/[CoO2]+
1200
1000
800
600
400
200
0
C60
Ar1000
Ar2000
Ar3000
(H2O)1200
Primary ions

(f)

FIG. 7. The effect of the primary ions C_{60}, Ar_n, $(CO_2)_n$ and $(H_2O)_n$ (n = 1000−3000) on the secondary ion yield ratio $[M_xO_yH_z]^+/[M_x]^+$ where M = metal from the samples MnO (a and b), NiO (c and d) and Co_3O_4 (e and f). The error bars represent the standard deviation of analysis obtained from two or three different areas.

Although the $(CO_2)_n$ GCIBs also provide a yield enhancement in $[MOH]^+/[M]^+$ similar in magnitude to that for $[MO]^+/[M]^+$, the enhancement in hydroxide adducts is much greater (~×100) when using the $(H_2O)_n$ GCIBs. However, the $[MOH]^+/[M]^+$ yield ratios observed from MnO and MnO_2 samples are quantitatively similar, suggesting these ion ratios are not appropriate for distinguishing the samples.

The $[MnO]^+/[Mn]^+$ yield ratios observed from MnO and MnO_2 samples are also influenced by the switch from $(Ar)_n$ to $(H_2O)_n$ GCIBs (Fig. S2). Consistent with the CO_2 cluster beams (Fig. 4), the largest $[MnO]^+/[Mn]^+$ signal ratio is observed with the largest, slowest $(H_2O)_n$ projectiles. It is noteworthy that for the same sized cluster (n = 3000) the SI yield ratios observed from both samples with the $(CO_2)_n$ beam is approximately twice that observed with the $(H_2O)_n$ projectile, which contains half as many oxygen atoms and is traveling with approximately twice the velocity - we have insufficient data to conclude whether this is significant from a mechanistic standpoint or purely coincidental.

IV. SUMMARY AND CONCLUSIONS

The surface and sub-surface of cobalt, manganese and nickel oxides were studied with ToF-SIMS using 70 keV GCIB projectiles. The relative SI yields $[M_xO_y]^+/[M_x]^+$ are influenced by GCIB projectile chemistry and to a lesser extent velocity (E/m). The

greatest SI yield ratios $[M_xO_y]^+/[M_x]^+$ are obtained with the largest,slowest clusters $(CO_2)_{3000}$. The cluster chemistry has a greater effect on the ratio $[M_2O_2]^+/[M_2]^+$ than on $[MO]^+/[M]^+$. For all GCIBs tested, steady-state ion ratios $[Mn_xO_y]^+/[Mn_x]^+$ reflect the oxidation state of manganese in the oxides studied. $(H_2O)_n$ GCIBs were found to increase the relative SI yields of hydroxide-containing and oxide species, compared with $(Ar)_n$ over the same (E/m) range. In contrast to the $[M_xO_y]^+$ data, the $[MOH]^+$ relative yields were found to not differ significantly between MnO and MnO_2 samples, implying these signals should not be used for speciation analysis. This observation may also provide information on the adduct ion formation process with reactive GCIBs, which will require further investigation. Future studies will explore the capabilities of high-energy GCIBs to speciate a wider range of metal oxide samples including lithium-ion batteries containing *NMC* cathodes.

ACKNOWLEDGMENTS

The authors gratefully acknowledge the UK Engineering and Physical Sciences Research Council (EPSRC) and the Henry Royce Institute for funding the instrumentation used in this work, including grants EP/S019863/1, EP/R00661X/1, EP/P025021/1 and EP/P025498/1. A.H.A. is funded through a studentship from the Saudi Arabia Cultural Bureau. We acknowledge M. Lagator for assistance with the ToF-SIMS.

AUTHOR DECLARATIONS

Conflicts of Interest

The authors have no conflicts to disclose.

DATA AVAILABILITY

The data that support the findings of this study are available from the corresponding author upon reasonable request.

REFERENCES

[1] T. Waldmann, A. Iturrondobeitia, M. Kasper, N. Ghanbari, F. Aguesse, E. Bekaert, L. Daniel, S. Genies, I. Jiménez Gordon, M. W. Löble, E. De Vito and M. Wohlfahrt-Mehrens, J. Electrochem. Soc. **163**, A2149 (2016).

[2] Y. Moryson, F. Walther, J. Sann, B. Mogwitz, S. Ahmed, S. Burkhardt, L. Chen, P. J. Klar, K. Volz, S. Fearn, M. Rohnke, and J. Janek, ACS Applied Energy Materials **4,** 7168 (2021).

[3] S. Marchesini, B. P. Reed, H. Jones, L. Matjacic, T. E. Rosser, Y. Zhou, B. Brennan, M. Tiddia, R. Jervis, M. J. Loveridge, R. Raccichini, J. Park, A. J. Wain, G. Hinds, I. S. Gilmore, A. G. Shard, and A. J. Pollard, ACS Applied Materials & Interfaces **14**, 52779 (2022).

[4] T.M. Brewer and L.T. Demoranville, Anal. Methods **4**, 3491 (2012).

[5] I. Yamada, J. Matsuo, N. Toyoda, A. Kirkpatrick, Mat. Sci. Eng. R **34**, 231(2001).

[6] S. Ninomiya, Y. Nakata, K. Ichiki, T. Seki, T. Aoki and J. Matsuo, Nucl. Instr. Meth. Phys. Res. B **256**, 493 (2007).

[7] Z. Postawa, R. Paruch, L. Rzeznik, and B. J. Garrison, Surf. Interface Anal. **45**, 35 (2013).

[8] J. L. S. Lee, S. Ninomiya, J. Matsuo, I. S. Gilmore, M. P Seah and A. G. Shard, Anal. Chem., **82**, 98 (2010).

[9] T. Miyayama, N. Sanada, S. R. Bryan, J. S. Hammond and M. Suzukia, Surf. Interface Anal. **42**, 1453 (2010).

[10] N. Gauthier, C. Courrèges, J. Demeaux, C. Tessier and H. Martinez, Appl. Surf. Sci. **501**, 144266 (2020).

[11] V. Winkler, G. Kilibarda, S. Schlabach, D. V. Szabó, T. Hanemann and M. Bruns, J. Phys. Chem. C **120**, 24706 (2016).

[12] Y. Yamagishi, H. Morita, Y. Nomura and E. Igaki, ACS Appl. Mater. Interfaces, **13**, 580 (2021).

[13] N. Winograd, Annu. Rev. Chim. Anal. Chem. **11**, 29 (2018).

[14] E. Cuynen, L. Van Vaeck and P. Van Espen, Rapid Commun. Mass Spectrom. **13**, 2287 (1999).

[15] M. Trzyna-Sowa, N. Berchenko, P. Dziawa and J. Cebulski, Appl. Surface Sci. **577**, 151855 (2022).

[16] A.J. Barlow, J. F. Portoles and P. J. Cumpson, J. Appl. Phys. **116**, 054908 (2014).

[17] S. Sheraz née Rabbani, I. Berrueta Razo, T. Kohn, N. P. Lockyer and J. C. Vickerman Anal. Chem. **87**, 2367 **(**2015).

[18] H. Tian, D. Maciążek, Z. Postawa,,B. J. Garrison and N. Winograd, J Am Soc Mass Spectrom. **30**, 476 (2019).

[19] S. J. Lee, A. Hong, J. Cho, C. M. Choi, J.Y. Baek, J.Y. Eo, B. J. Cha, W. J. Byeon, J. Y. We, S. Hyun, M. Jeon, C. Jeon, D. J. Ku and M. C. Choi, Appl. Surface Sci., **572**, 151467 (2022).

[20] J.S. Fletcher, S. Rabbani, A. Henderson, P. Blenkinsopp, S. P. Thompson, N. P. Lockyer and J. C. Vickerman, Anal. Chem., **80**, 9058 (2008).

[21] N. G. Korobeishchikov, I. V. Nikolaev, M. A. Roenko and V. V. Atuchin, Appl. Phys. A **124**, 833 (2018).

[22] P. J. Cumpson, J. F. Portoles, A. J. Barlow and N. Sano, J. Appl. Phys. **114**, 124313 (2013).